IEEE Access
Multidisciplinary | Rapid Review | Open Access Journal

Received April 1, 2020, accepted April 29, 2020, date of publication May 14, 2020, date of current version June 1, 2020.

Digital Object Identifier 10.1109/ACCESS.2020.2994358

An Implantable Wideband Microstrip Patch Antenna Based on High-Loss Property of Human Tissue

ZHI-JIE YANG[1], (Member, IEEE), LEI ZHU[2], (Fellow, IEEE), AND SHAOQIU XIAO[1], (Member, IEEE)

[1]School of Physics, Institute of Applied Physics, University of Electronic Science and Technology of China, Chengdu 610054, China
[2]Department of Electrical and Computer Engineering, Faculty of Science and Technology, University of Macao, Macau

Corresponding author: Shaoqiu Xiao (xiaoshaoqiu@uestc.edu.cn)

This work was supported in part by the National Natural Science Foundation of China under Grant 61731005 and Grant 61971475, in part by the University of Macau under Muki-Year Grant MYRG2017-00007-FST and Grant MYRG2018-00073-FST, in part by the Special under Grant CPG2019-00024-FST, and in part by the Fundamental Research Funds for the Central Universities under Grant ZYGX2016Z008.

ABSTRACT In this paper, an approach was designed to develop an implantable wideband microstrip patch antenna (MPA) by the high-loss property of human tissue. In order to reduce the detuning effect, an extensive investigation was conducted, demonstrating the effects of high-loss human tissue on the total quality factor (Q_T), effective relative permittivity, and effective loss tangent of the deeply implanted MPA. To the best of our knowledge, the exact three parameters for the deeply implanted MPA are firstly studied. From the evolutionary point of view, a deeply implanted MPA can be treated as a resonator with the extremely low and stable Q_T. As such, its wide impedance bandwidth can be easily achieved through two inherent radiative modes of the embedded MPA under the high-loss environment. Finally, the proposed MPA will be fabricated and tested, and the final outcomes are consistent with the corresponding simulated results.

INDEX TERMS Implantable microstrip patch antenna, high loss, human tissue, wideband impedance bandwidth.

I. INTRODUCTION

Recently, there is an increasing interest in designing and developing the wirelessly linked implantable medical devices (IMDs) for its applications in diagnosis and treatment towards effective communication with in-vitro monitors [1], [2]. An implantable antenna is generally taken as a key component of the biotelemetry system. Many kinds of the designed antennas can be embedded into human body, such as dipole [3]–[8], loop [9]–[11], helix [12], [13], microstrip patch antenna (MPA) [14]–[26], etc. Compared with other antennas, MPA is highly preferred for its easy fabrication, low profile, and integration with other electronic devices [14], [15].

The essential requirement for an implantable antenna is its stability of the resonant performance in human tissue. The performance of an implantable antenna strongly depends on the individuals' anatomical features of the surrounding tissues [7], [27]. Meanwhile, the dielectric properties of human tissue may be changed with multiple factors, such as gender, age, weight [7], etc. Thus, the detuning effect was identified as a great challenge for the design of an implantable antenna [28]. In general, a broadband impedance matching is highly demanded to compensate for an uncontrollable frequency shift [26]–[28].

So far, several research groups have made great significant contributions to design works of the wideband implantable MPAs. First of all, the impedance bandwidth of MPA is improved by the increased thickness of the substrate [29]. However, the intrinsic low-profile of MPA would be destroyed, resulting in the discomforts of patients. Besides, there are disadvantages of the limited bandwidth and the increased height of the antenna. Secondly, the additional resonant modes are proven to be effective. A variety of slots etched on the patch and ground [15]–[19], parasitic and stacked patches [20]–[26] are used to excite the non-inherent modes under its dominant radiative mode [30]. Reports show that the widest impedance bandwidth of an implantable

The associate editor coordinating the review of this manuscript and approving it for publication was Cihun-Siyong Gong.

This work is licensed under a Creative Commons Attribution 4.0 License. For more information, see https://creativecommons.org/licenses/by/4.0/

MPA may reach up to about 47% through etching an open-end slot on the ground [17]. However, the radiation patterns of the additional modes may be substantially changed with frequency and suffer from high cross-polarization [30]. To sum up, most of the published works are focused on broadening the impedance bandwidth of the antennas, but any insight into human tissue has not been comprehensively taken. Previously, the implantable MPAs with broadband performance are designed for shallow implantation, for instance, less than 5 mm of thickness, and low-frequency band (i.e., 400 MHz). In this paper, a design methodology based on the high-loss property of human tissues is firstly proposed to cope with the detuning effect for the deeply implanted MPA with the resonance of 2.4 GHz.

In Section II, the quantitative analysis is used to study the impaction of the high loss radiation environment on MPA. Except for effective relative permittivity (ε_{er}) and effective loss tangent ($\tan\delta_e$), the total quality factor (Q_T) of the deeply implanted MPA can be determined. Three important factors of implantation depth are investigated, demonstrating the stability of the embedded MPA in human tissue. To the best of our knowledge, the basic design theory about the deeply implanted MPA is firstly introduced to broaden the impedance bandwidth. In Section III, a differential-fed MPA with its distinctive Q_T and input impedance is designed to monitor the pacemaker through the high-loss property of human tissue. In addition, the dual-band radiated modes are created for an implantable MPA with wide bandwidth. Sensitivity analysis was further carried out in terms of the different implantation depth, conductivity, and relative permittivity. Then the model integrity is studied to evaluate the practicality of the proposed MPA. In Section IV, the examination results of the fabricated antenna are accessible for the simulations. The conclusion can be eventually drawn in Section V.

II. PROPERTIES OF HUMAN TISSUE FOR IMPLANTABLE MPA

The goal of our work was to quantify the impaction of human tissue on the embedded MPA and increase its functional performances. To be specific, the total quality factor (Q_T), effective relative permittivity (ε_r), and effective loss tangent ($\tan\delta_e$) of MPA in human tissue would be analyzed. First and foremost, the implantable antenna played a key role in the wireless communication between IMDs and in-vitro monitors. Thus, the implantable MPA and practical IMD should be jointly designed [31]–[34]. Herein, the metal case of the pacemaker was taken as the ground plane of the proposed MPA [31], [34]. Fig.1 illustrates the entire geometry of a pacemaker with the addition of an implantable MPA. The size of the pacemaker was 40 mm × 40 mm ×10 mm, as it was referred from [33], [34].

Next, the embedded environment of IMDs might produce a significant effect on the performance of the implantable antenna, which was totally different from free-space. The radiated region of an in-body antenna referred to human tissue of which the heterogeneous media consisted of multiple

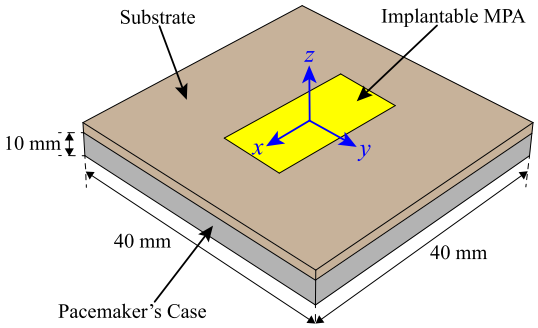

FIGURE 1. Illustration of a pacemaker integrated with MPA.

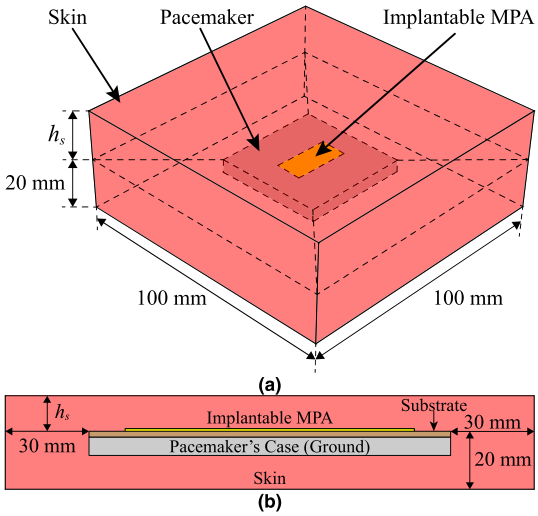

FIGURE 2. (a) Cubic skin model for a pacemaker assembled with implantable MPA, and (b) Side view of (a).

layers of tissue with frequency-dependent dielectric properties [27], [28]. In order to quantitatively analyze the influence of human tissue on the antenna, a useful model based on a single-layered tissue was utilized [1], [2]. Consequently, a frequency-dependent one-layered skin model [14] could be obtained, as it is shown in Fig. 2. The pacemaker with an implantable MPA was embedded in the center of this skin model. The distance from the structural side to the edge of the skin model was 30 mm at both sides. The distance from MPA to the bottom of the skin model was 20 mm. Then our proposed MPA was embedded in this tissue model with a depth of h_s; meanwhile, its upper surface was oriented towards the skin surface. The size of the cubic skin model was set as 100 mm × 100 mm × $(20 + h_s)$ mm.

A. Q_T OF IMPLANTABLE MPA

As it was mentioned above, the increase of impedance bandwidth was an effective approach to antagonize the detuning effect. Since Q_T was inversely proportional to impedance bandwidth, the relationship between Q_T and impedance bandwidth (BW) could be expressed as follows [29]:

$$BW = (VSWR - 1) \Big/ \left(Q_T \sqrt{VSWR}\right) \tag{1}$$

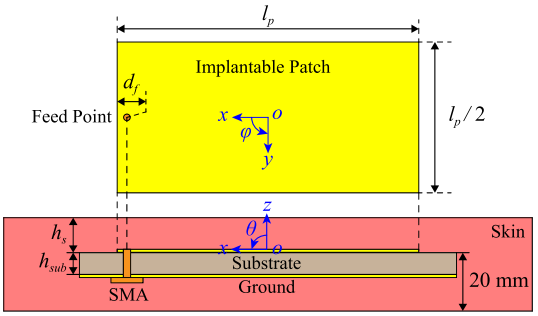

FIGURE 3. Physical simulation model of the implantable MPA.

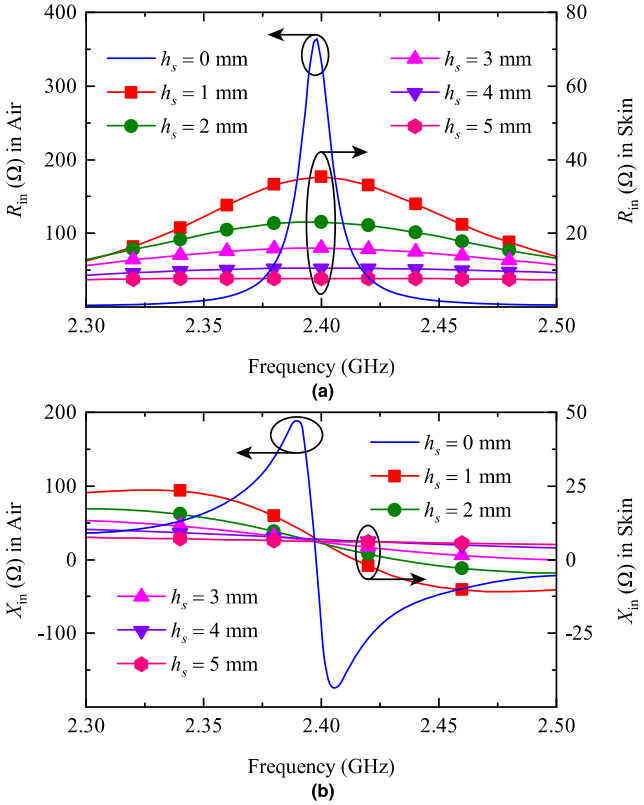

FIGURE 4. Simulated input impedance of shallow implanted MPA: (a) R_{in}, (b) X_{in}.

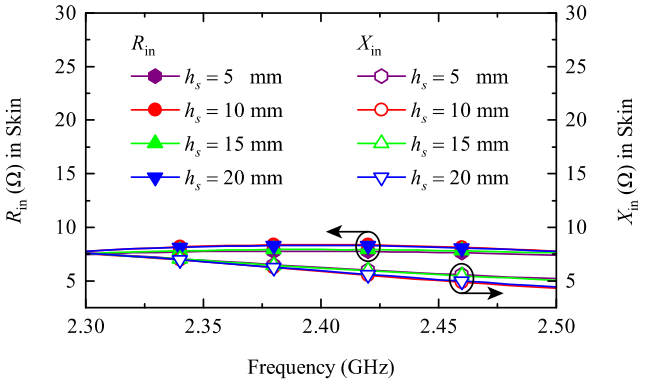

FIGURE 5. Simulated input impedance of deep implanted MPA.

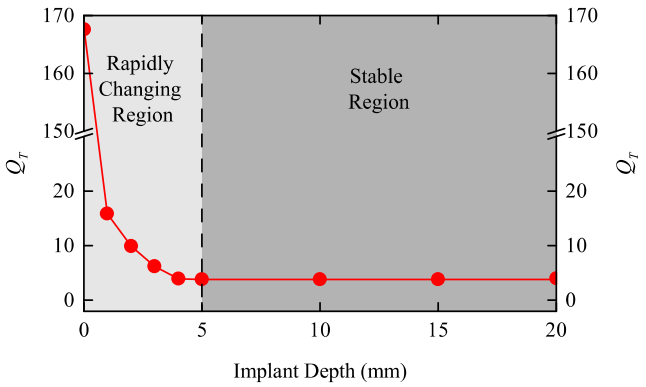

FIGURE 6. Simulated Q_T with respect to different h_s.

where *VSWR* is the voltage standing-wave ratio and usually 2:1.

Thus, it is figured out that Q_T is the critical factor of broadening the impedance bandwidth of MPA. Generally, Q_T could be reduced by thickening the substrate, etching slots on the patch and ground. However, more attention was paid to the design of an antenna itself. Few works were reported to make quantitative analysis about the influence of the surrounding environment on the implantable MPA. In this study, these influence factors should be elaborated in the design of the implantable MPA.

The physical model of the implantable MPA is illustrated in Fig. 3. In this model, the case of the pacemaker was acted as the reflector with the thickness of 0 mm. Through the simplified calculation process, our attention could be paid to study the influence of human tissue on the performance of the implantable MPA. In fact, the size of the case was electrically large enough to suppress the edge effect of MPA. As a result, the thickness of the ground produced little effect on the radiation performance [35]. It was supposed that an infinitely thin ground was used. The simplified model was composed of a traditional MPA for being embedded into the skin. The MPA itself was printed on Rogers RO6010 with the thickness of $h_{sub} = 0.635$ mm and the resonance of 2.4 GHz. Unless otherwise specified, all of the proposed MPAs used the same thickness of the substrate. In Fig. 3, l_p is the physical length of the non-radiation edge while the length of the radiation edge is only one half of l_p. MPA was directly fed by a 50 Ω coaxial probe near the radiated edge. d_f was the distance between the center of the coaxial probe and the edge, i.e., 0.5 mm.

According to [6] and [35]–[37], Q_T could be obtained by the following formula:

$$Q_T(\omega_0) = \left[\frac{\omega_0}{2R_{in}(\omega_0)}\right]\sqrt{\left[R'_{in}(\omega_0)\right]^2 + \left[X'_{in}(\omega_0) + \frac{X_{in}(\omega_0)}{\omega_0}\right]^2} \tag{2}$$

where ω_0 is the radian frequency; $\omega_0 = 2\pi f$; f is the working frequency. $R_{in}(\omega_0)$ and $X_{in}(\omega_0)$ are the input resistance and reactance of MPA; $R'_{in}(\omega_0)$ and $X'_{in}(\omega_0)$ are the corresponding slopes. Thus, Q_T could be expressed by the input impedance of MPA; in addition, the required four parameters could be simulated by HFSS.

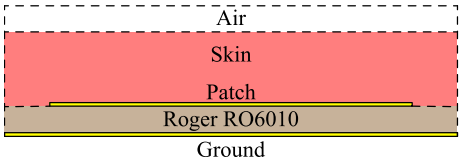

FIGURE 7. Cross-sectional view of conventional MPA with loaded skin.

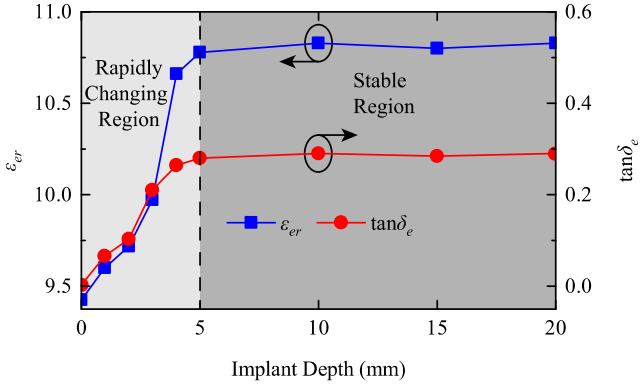

FIGURE 8. The effective parameters, ε_{er} and tanδ_e, with respect to different h_s.

B. DISCUSSION OF THE RESULTS

The required parameters on the right side of Eq. (2) are shown in Fig. 4 and Fig. 5, respectively. In this paper, the calculation process was divided into two stages: shallow implantation ($h_s \leq 5$ mm), and deep implantation ($h_s > 5$ mm). Fig. 4(a) and Fig. 4(b) illustrate the calculated input impedance of the shallowly implanted MPA and those of the deeply implanted MPA in Fig. 5. The input impedance is dramatically reduced with the increasing implantation depth (h_s) in Fig. 4, which are almost the same in Fig. 5. While substituting the required values in Eq. (2), the desired Q_T with different implantation depths could be obtained in Fig. 6. In order to ensure the consistency of the skin with frequency-dependent dielectric properties, f was readily fixed at 2.4 GHz. As it could be seen in Fig. 6, Q_T was substantially decreased with the depth h_s of MPA in the rapidly varied region (shallow implantation, $h_s \leq 5$ mm). In the stable region (deep implantation, $h_s > 5$ mm), Q_T was almost identical. Results indicated that the deeply implanted MPA was actually a lossy resonator with extremely low and stable Q_T, which might be totally different from those of other conventional MPAs in the air with high Q_T.

In general, the extremely low and stable Q_T was generated by the huge loss of the loaded skin. As it is shown in Fig. 7, a standard MPA is produced with loading of a high loss superstrate when MPA is embedded into human tissue. Q_T could be calculated by four types of losses [35] as follows:

$$1/Q_T = (1/Q_r) + (1/Q_d) + (1/Q_c) + (1/Q_s) \quad (3)$$

It was acknowledged that the surface-wave loss Q_s could be generally neglected in the thin substrate; the conductor loss Q_c was a constant; the radiation loss Q_r was determined by the thickness and ε_{er}; the dielectric loss Q_d was inversely proportional to the loss tangent tanδ_e. The detailed calculation process for ε_{er}, tanδ_e, and Q_T in the shallowly implanted MPA ($h_s \leq 4$ mm) were reported in [35]. The influence of human tissue on the deeply implanted MPA ($h_s > 5$ mm) had never been reported before. Therefore, a quantitative study about the deeply implanted MPA was performed in this paper. Fig. 8 indicates the obtained values of ε_{er} and tanδ_e. Similarly, ε_{er} and tanδ_e were stable in the deeply implanted MPA. In contrast to tanδ_e in the air, the corresponding value in the skin was sharply increased. The dominant factor Q_T was changed from Q_r to Q_d, and related values were determined by tanδ_e. In this paper, the high-loss properties of human tissue were primarily introduced for the design of an implantable wideband MPA.

The stable input impedance, ε_{er}, tanδ_e, and Q_T in deep implantation brought an interesting point of view in the design of implantable antennas. According to Eq. (1), it can be well understood that Q_T is opposite to impedance bandwidth. From Fig. 6, Q_T is dramatically reduced with the increasing implantation depth in the shallowly implanted MPA. Thus, to increase the implantation depth is an easy approach to broaden the impedance bandwidth of the implantable MPA ($h_s \leq 5$ mm). Due to the stable Q_T, there was an intrinsic limitation for deep implantation, that was, how to further broaden the impedance bandwidth. In this context, the high-loss property with the extremely low and stable Q_T allowed the slow variation of the input impedance of the implantable MPA in human tissue within the desired operating band so that the inherent radiated modes could be facilely excited. Therefore, the so-called detuning effect might be effectively solved under the wideband performance of the implantable MPA.

Typically, the pacemaker was implanted with a depth of about 25.4 mm under the skin surface [2] so that the above-mentioned characteristic could be stably maintained. However, the implantation depth of IMD in millimeters could hardly be controlled in current medical conditions. Thus, the tolerance to the variation of implantation depth should be further investigated for the implantable MPA in human tissue. As it was mentioned above, the deeply implanted MAP could be developed in a similar way.

III. ANTENNA DESIGN AND PARAMETRIC STUDY

Our next target is to design an implantable MPA in the deep implantation with wide impedance bandwidth that overcomes the detuning effect by means of the inherent high loss properties of human tissue. The proposed MPA can be operated at the 2.4-2.48 GHz industrial, scientific, and medical (ISM) band. Fig. 9 shows the geometrical schematic of the proposed differential-fed MPA with the detailed parameters, as denoted in Table 1. For convenience of application, the origin of the coordinate system serves as the center of the implantable MPA. It can be seen from Fig. 9 that a pair of 50 Ω coaxial probe with equal amplitude and 180° phase difference [30], [38] is installed to feed this MPA with a pair of one-quarter-wavelength impedance transformer. The proposed MPA is implanted in the one-layered skin model with 20 mm

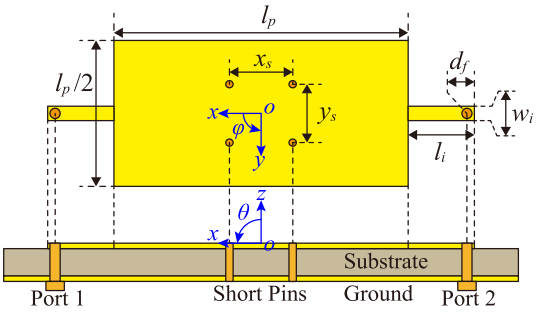

FIGURE 9. Geometrical schematic of the proposed implantable MPA.

TABLE 1. Detailed dimensions of proposed MPA in Fig. 9.

Parameters	l_p	l_i	w_i	x_s	y_s	d_f
Value (mm)	20	4.5	1	8.6	4	0.5

embedded depth, as indicated in Fig. 2. Here, the used substrate is still Rogers RO6010 with a thickness of 0.635 mm.

A. OPERATING PRINCIPLE

In order to communicate with in-vitro monitor, the radiation peak of the proposed MPA should be kept at boresight. The differential signals can effectively suppress those even-order modes, e.g., TM_{20} and TM_{22}, with null in broadside direction. Meanwhile, the length of the edge was adjusted in order to remove the TM_{12} mode out of the operating band. The process of removing or suppressing those undesired modes has been extensively reported in [30]. As a sequence, only TM_{10} and TM_{30} modes were resonated in the operation range.

According to the discussion in Section II, the input impedance of the deeply implanted MPA had a very small value and a smooth variation, making this property useful for impedance matching. Then, a pair of microstrip line was introduced to feed this MPA. Fig. 10 illustrates the simulated R_{in} of a differential-driven implanted MPA with different lengths of microstrip line (l_i). From Fig. 10, it can be seen that the resonant frequency of TM_{30} mode (f_{30}) tends to decrease with the lengthening l_i, and the corresponding value of TM_{10} mode (f_{10}) remains approximately constant. In Fig. 11, the radiated patch with the reflected ground is connected by the two pairs of short pin in the diameter of 0.5 mm. By widening the distance between the two pairs of short pin (x_s), f_{10} was increased, and the R_{in} between the TM_{10} and TM_{30} modes was raised. In such a way, good impedance matching around the designed frequency can be achieved by the input impedance of the proposed MPA.

B. SIMULATED RESULTS

The simulated reflection coefficient ($|S_{dd11}|$) [30] of the differential-driven implantable MPA is shown in Fig. 12. In Fig. 12, there is the emergence of the two distant radiated modes, i.e., TM_{10} and TM_{30} modes. To the greatest extent, the simulated $|S_{dd11}|$ bandwidth below -10 dB was ranged from 2.09 and 4.14 GHz (65.8% infraction). The broad bandwidth was achieved by means of the tissue's impaction on deeply implanted MPA. Fig. 13 and Fig. 14 show the realized gain

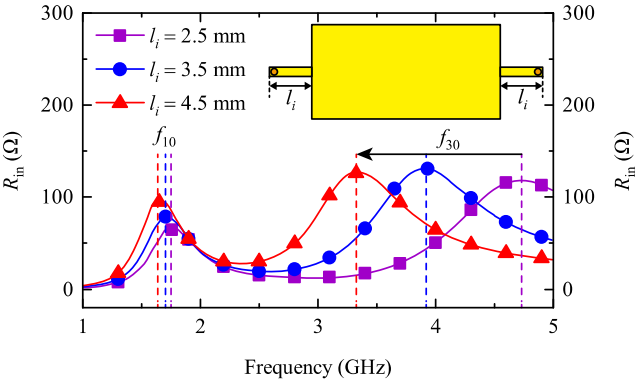

FIGURE 10. Simulated R_{in} of differential-driven implanted MPA with different l_i.

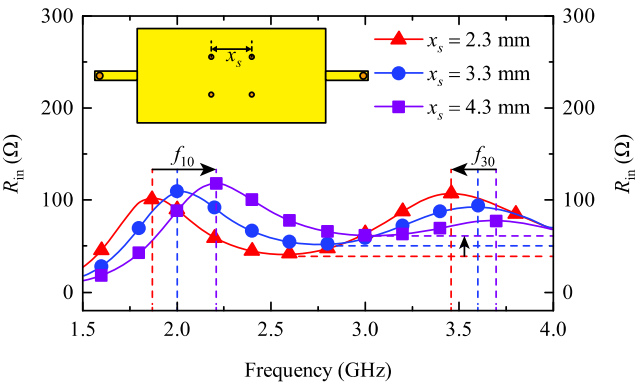

FIGURE 11. Simulated R_{in} of differential-driven implanted MPA with different x_s.

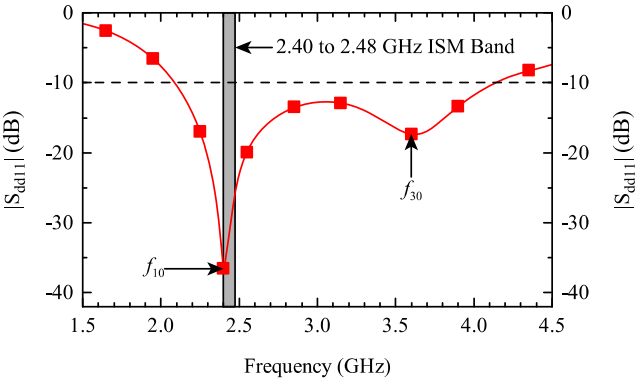

FIGURE 12. Simulated $|S_{dd11}|$ of the proposed MPA.

patterns at two resonant modes, including 2.41 and 3.61 GHz. The proposed MPA had a peak gain of −17.3 dBi and was radiated in the Z-axis direction. The high loss of the surrounding human tissue made contributions to the negative gain. With four planes, the co-polarizations were symmetrical and the cross-polarization suppression was suppressed lower than -46 dBi, respectively.

As for designing the implantable equipment, people's safety should be the largest issue. To realize such a goal, the IEEE standard of C95.1-1999 and C95.1-2005 not only assessed the RF radiation safety but also set a restriction on the specific absorption rate (SAR) levels [20]. In other words, two standards should be observed by all the designed implantable antenna. The standard of C95.1-1999 restricts

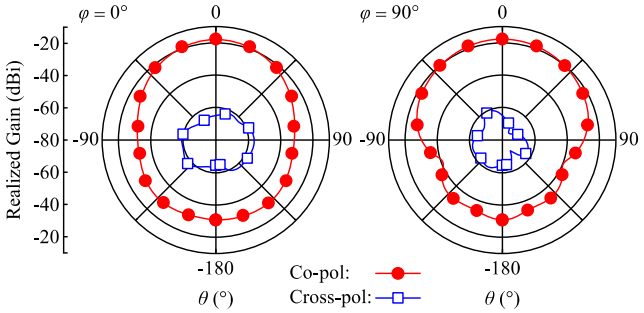

FIGURE 13. Simulated realized gain patterns of the designed MPA in the *XZ*- and *YZ*-plane at 2.41 GHz.

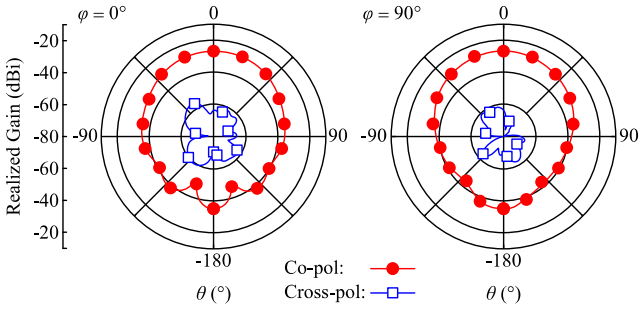

FIGURE 14. Simulated realized gain patterns of the designed MPA in the *XZ*- and *YZ*-plane at 3.61 GHz.

that the SAR levels averaged over 1-g of human tissue should be less than 1.6 W/kg, while the standard of C95.1-2005 indicates that the SAR levels averaged over 10-g of tissue should be less than 2 W/kg. The former standard was applied in this work since the standard of C95.1-1999 is much tougher than that of the C95.1-2005. The simulated value of maximum averaged SAR in 1-g of human skin at 2.4 GHz was presented by the first column of Table 2, which will be 226.5 W/kg if the input power was 1 W. To observe with the standard of IEEE standards of C95.1-1999, the maximum input power of the proposed MPA should be less than 9.5 mW in one-layered skin model, as it was shown in the third column of Table 2.

C. SENSITIVITY ANALYSIS

As it was mentioned above, an implantable antenna was always embedded in human tissue, which makes its resonant performance primarily dependent on the surrounding tissue. As a result, the antenna's resonance under various tissue-loading conditions should be investigated in order to make a right evaluation, i.e., relative permittivity (ε_r), implant depth (h_s), and conductivity (σ).

On the one hand, there are different dielectric properties of human tissue, enabling the performances of implantable antennas to be largely influenced by tissue variations. To quantitatively evaluate the proposed MPA, the ε_r and σ of skin have been changed from 50% to 150%, and the simulated results are shown in Fig. 15 and Fig. 16, respectively.

When the ε_r was increased, the resonant frequency would be shifted to a lower band, as shown in Fig. 15. Meanwhile, it is shown in Fig. 16 that the σ has little impact on the resonant frequency. Besides, the relationship between the

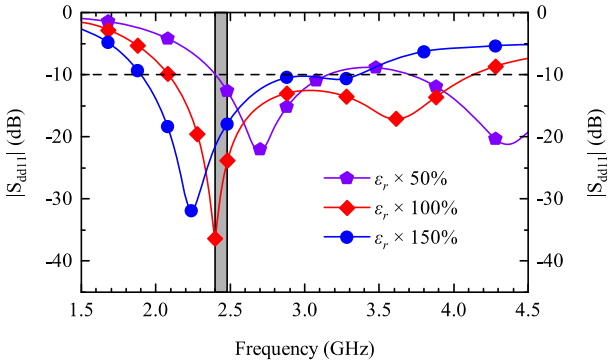

FIGURE 15. Simulated $|S_{dd11}|$ as ε_r of skin varies by ±50%.

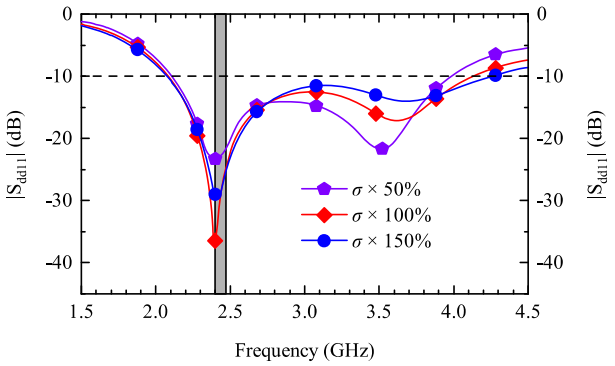

FIGURE 16. Simulated $|S_{dd11}|$ as σ of skin varies by ±50%.

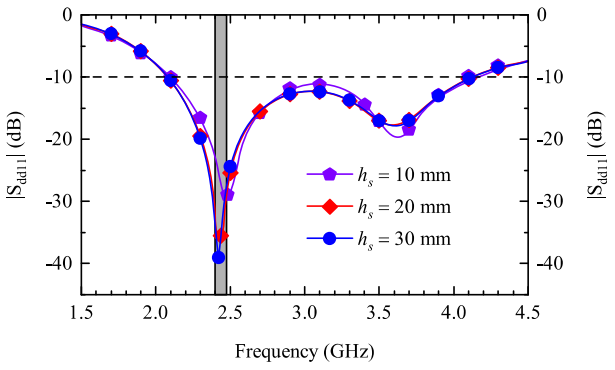

FIGURE 17. Simulated $|S_{dd11}|$ as h_s varies by ±10 mm.

TABLE 2. Maximum SAR values (input power = 1 W) and maximum allowed input power for the proposed antenna in one-layered skin model.

Maximum SAR (W/kg)		Maximum allowed net-input power (mW)	
1-g avg	10-g avg	C95.1-1999	C95.1-2005
226.5	38.5	9.5	48.1

working frequency and ε_r could be written as [29]

$$f = c/\left(2l_p\sqrt{\varepsilon_r}\right) \tag{4}$$

where the f stands for the working frequency, c refers to the speed of light, and l_p represents the physical length of MPA.

From Eq. (4), it can be seen that the f is inversely proportional to ε_r when l_p and c are constants, which are well consistent with the phenomenon in Fig 15. According to Eq. (4), the working frequency of MPA could not be directly

affected by the σ, as shown in Fig. 16. Moreover, there were obvious variations in impedance matching when the ε_r and σ of skin were changed from 50% to 150%. In fact, both of the ε_r and σ have a huge influence on the tanδ of skin. Thus, the relationship among these three parameters can be deduced as

$$\tan\delta = \sigma \big/ \omega\varepsilon_0\varepsilon_r \tag{5}$$

where $\omega = 2\pi f$ is the radian frequency.

In Fig. 4 and Fig. 5, the MPA impedance is reduced with the increased implant depth, which can decide the drastic decline of Q_T in human tissue, shown in Eq. (2). In [35], it was proved that the most important factor of the steep fall of the Q_T was brought about by the tanδ of human tissue. That was the reason why the variations of ε_r and σ can effectively affect the impedance matching with the tanδ.

Moreover, the embedded location might be changed with human tissue activities and posture movement even if an implantable antenna was designed for a specific IMD. Fig. 17 illustrates the simulated $|S_{dd11}|$ with different h_s. It can be seen that there are almost the same resonant responses with different h_s, which are consistent with the phenomenon in Fig. 6 and Fig. 8.

Even though the variations of the dielectric properties (50%) and implant depth (10 mm) of the tissue were larger than those reported in the past, it was found out that the impedance bandwidth of the proposed antenna cloud cover the desired 2.4 GHz ISM band. It is suggested that the proposed MPA had better tolerance to the diversity of human tissue than other reported ones. In addition, the maximized impedance bandwidth can lead to the impressive stabilities of the proposed MPA to various properties of tissue, as discussed above.

D. MODEL INTEGRITY STUDY

As it was mentioned above, the quantitative analysis was realized by the simplified human tissue model and the pacemaker model. Besides, the human tissue was simplified as the one-layered skin model. In addition, the thickness of the pacemaker case or virtual ground plane was set as 0 mm. Practically, the actual IMDs should be used to design the implantable antenna. To realize the performance of the designed MPA assembled with the realistic pacemaker model in the human body, more and more complicated models should be shown in Fig. 18(a) and Fig. 18(b), respectively.

The pacemaker in Fig. 18(a) was modeled as a hollow closed metal (titanium) cavity filled with electronic components, i.e., battery and circuitry. The size of the pacemaker was 40 mm × 40 mm, the thickness of the whole case was set as 10 mm, and the proposed MPA was still printed on the Rogers RO6010 with a thickness of 0.635 mm. Previously, the chest of the Gustav or anatomical human body model places this complicated pacemaker model, as shown in Fig. 18(b), which is also labeled as 'complete model' in Fig. 19. What is more, the proposed MPA in the past with infinitely thin ground embedded in the one-layered skin model is marked as the 'simplified model'. From Fig. 19, it

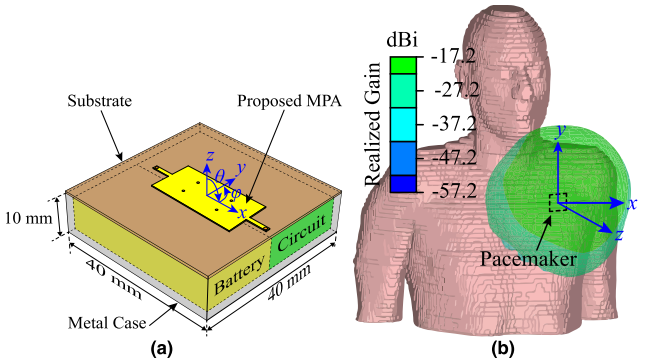

FIGURE 18. (a) Complete pacemaker model, and (b) anatomical human body model.

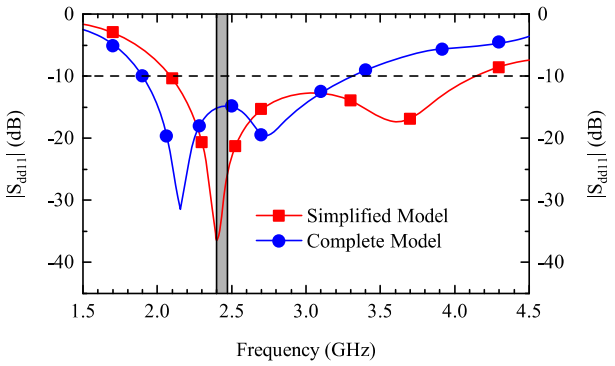

FIGURE 19. Simulated $|S_{dd11}|$ in different models.

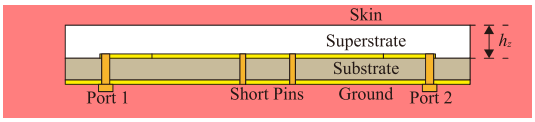

FIGURE 20. Schematic geometry of the proposed MPA coating with zirconium.

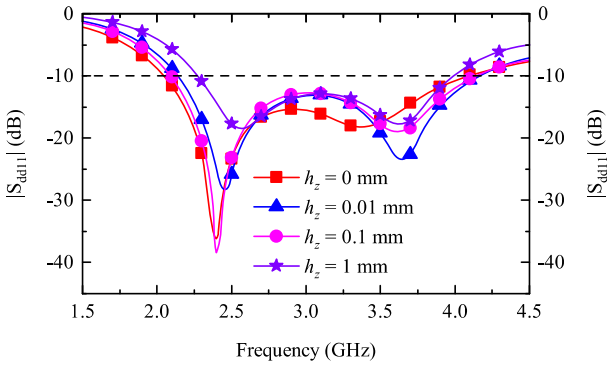

FIGURE 21. Simulated $|S_{dd11}|$ of the proposed MPA with different thickness of zirconium.

is seen that the complete model and its two resonant modes still have good resonant performance in the desired operating frequency band.

E. BIOCOMPATIBLE MATERIALS STUDIES

Biologically, the implantable antennas should not only prevent rejection of the implant but also preserve patient safety [1]. Previously, the proposed MPA was directly exposed to the tissue. It was a useful method to insulate the

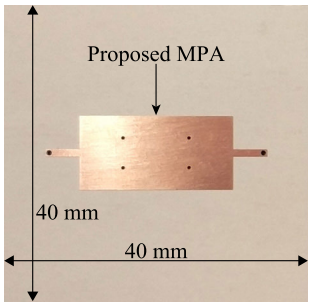

FIGURE 22. Photograph of the fabricated implantable MPA.

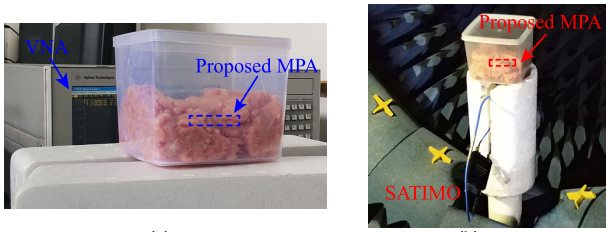

FIGURE 23. Photographs of experimental set-up for measuring the proposed MPA: (a) vector network analyzer, (b) SATIMO near-field antenna measurement system.

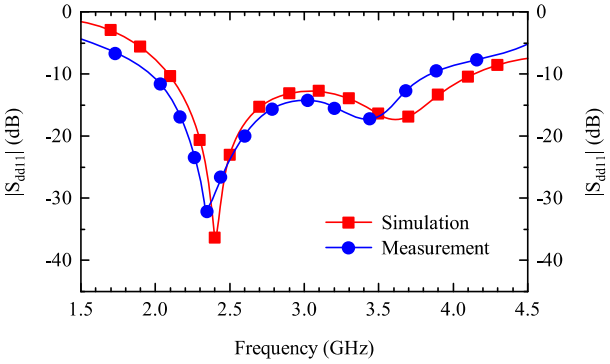

FIGURE 24. Simulated and measured $|S_{dd11}|$ of the porposed MPA in the pork.

implantable MPA with a layer of biocompatible coating [1], which made it easy to divide human tissue from direct contacting to implantable devices. Accordingly, zirconium with thin was chosen as the biocompatible superstrate. Fig. 20 shows the schematic geometry of the proposed MPA coating with zirconium. The thickness of the zirconium was marked as h_z. The simulated $|S_{dd11}|$ of the proposed MPA with different thickness of zirconium is shown in Fig. 21. The $h_z = 0$ mm is an indication that the MPA works in the skin with no superstrate. Fig. 21 shows that there is a wide impedance bandwidth in the proposed MPA with a superstrate.

IV. MEASURED RESULTS

Fig. 22 and Fig. 23 show the photographs of the fabricated MPA and the experimental facilities, respectively. From Fig. 22, it is seen that the proposed MPA is fabricated on the basis of the simplified model. The proposed MPA was characterized through implanting it in the depth of $h_s = 20$ mm

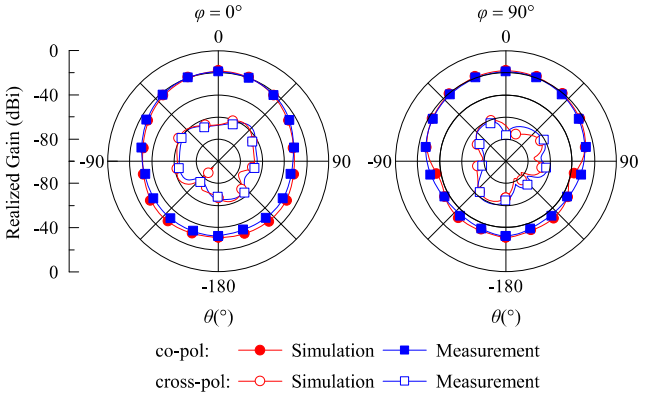

FIGURE 25. Realized gain patterns of the simulation and measurement at the first resonant frequency of porposed MPA.

inside minced-pork [14], [20], and [22]. Its performance was experimentally confirmed, as shown in Fig. 23.

The pork with an overall dimension of 100 mm × 100 mm × 80 mm was housed by a plastic container. The dual-ports of the differential-driven MPA with equal amplitude and 180° phase difference [30], [38] was fed with a wideband power divider. The vector network analyzer (VNA) and SATIMO near-field antenna measurement system were used to get the measured $|S_{dd11}|$ and realize gain patterns of the proposed antenna. In addition, the measurement environment was kept at the ambient temperature of 25 °C, among which 60% was relatively humid.

Fig. 24 shows the measured and simulated results of $|S_{dd11}|$, accompanied by the photographs of the fabricated prototype of the proposed MPA and the VNA. Nevertheless, it is easy to observe the two resonant modes. Fig. 25 shows the normalized realized gain patterns of simulation and measurement at the first resonant frequency with the photograph of the fabricated MPA in SATIMO. Good agreement between the measured and simulated results is achieved. Besides, some uncertain or unexpected factors can lead to a small amount of variations in the measured results, including measurement tolerance and manufacturing irregularities.

V. CONCLUSION

By fully utilizing the properties of the human tissue in deep implantation to overcome the detuning effect, a design approach is used for the first time to design the implantable microstrip patch antennas in this paper. The influence of the surrounding tissue on the deeply implanted MPA is quantified. Specifically, the Q_T of deeply implanted MPA is calculated from the input impedance. Two important parameters, i.e., input impedance and Q_T, of MPA, are found to remain unchanged with an extremely low value in deep implantation. Firstly, a robust resonant performance of implantable MPA is realized owing to its stabilities in deep implantation. Secondly, an implantable differential-driven MPA based on dual-radiative modes is designed, fabricated, and tested through fully applying the inherent high-loss feature of human tissue, which is helpful to break the limit of the stable and low Q_T coming from the influence of human tissue. What is

more, the proposed MPA has achieved much wide impedance bandwidth. Next, the sensitivity analysis of the embedded environment is an indication that MPA has an impressive tolerance to various properties of human tissue. The correctness of the proposed theory has been proved based on the model integrity alternatively. In addition, it is found that the simulated results are in agreement with the measured ones.

REFERENCES

[1] A. Kiourti and K. S. Nikita, "A review of implantable patch antennas for biomedical telemetry: Challenges and solutions [Wireless Corner]," *IEEE Antennas Propag. Mag.*, vol. 54, no. 3, pp. 210–228, Jun. 2012.
[2] E. Chow, M. Morris, and P. Irazoqui, "Implantable RF medical devices: The benefits of high-speed communication and much greater communication distances in biomedical applications," *IEEE Microw. Mag.*, vol. 14, no. 4, pp. 64–73, Jun. 2013.
[3] H.-Y. Lin, M. Takahashi, K. Saito, and K. Ito, "Performance of implantable folded dipole antenna for in-body wireless communication," *IEEE Trans. Antennas Propag.*, vol. 61, no. 3, pp. 1363–1370, Mar. 2013.
[4] L.-J. Xu, Y.-X. Guo, and W. Wu, "Miniaturized dual-band antenna for implantable wireless communications," *IEEE Antennas Wireless Propag. Lett.*, vol. 13, pp. 1160–1163, 2014.
[5] V. T. Nguyen and C. W. Jung, "Radiation-pattern reconfigurable antenna for medical implants in MedRadio band," *IEEE Antennas Wireless Propag. Lett.*, vol. 15, pp. 106–109, 2016.
[6] S. Bakogianni and S. Koulouridis, "On the design of miniature MedRadio implantable antennas," *IEEE Trans. Antennas Propag.*, vol. 65, no. 7, pp. 3447–3455, Jul. 2017.
[7] M. K. Magill, G. A. Conway, and W. G. Scanlon, "Tissue-independent implantable antenna for in-body communications at 2.36–2.5 GHz," *IEEE Trans. Antennas Propag.*, vol. 65, no. 9, pp. 4406–4417, Sep. 2017.
[8] Y. Li, Y.-X. Guo, and S. Xiao, "Orientation insensitive antenna with polarization diversity for wireless capsule endoscope system," *IEEE Trans. Antennas Propag.*, vol. 65, no. 7, pp. 3738–3743, Jul. 2017.
[9] L.-J. Xu, Y.-X. Guo, and W. Wu, "Miniaturized circularly polarized loop antenna for biomedical applications," *IEEE Trans. Antennas Propag.*, vol. 63, no. 3, pp. 922–930, Mar. 2015.
[10] M. W. A. Khan, M. Rizwan, L. Sydanheimo, T. Bjorninen, Y. Rahmat-Samii, and L. Ukkonen, "Characterization of 3-D loop antenna to overcome the impact of small lateral misalignment in wirelessly powered intracranial pressure monitoring system," *IEEE Trans. Antennas Propag.*, vol. 65, no. 12, pp. 7405–7410, Dec. 2017.
[11] L.-J. Xu, B. Li, M. Zhang, and Y. Bo, "Conformal MIMO loop antenna for ingestible," *Electron. Lett.*, vol. 53, no. 23, pp. 1506–1507, Oct. 2017.
[12] O. H. Murphy, C. N. McLeod, M. Navaratnarajah, M. Yacoub, and C. Toumazou, "A pseudo-normal-mode helical antenna for use with deeply implanted wireless sensors," *IEEE Trans. Antennas Propag.*, vol. 60, no. 2, pp. 1135–1139, Feb. 2012.
[13] C. Liu, Y.-X. Guo, and S. Xiao, "Circularly polarized helical antenna for ISM-band ingestible capsule endoscope systems," *IEEE Trans. Antennas Propag.*, vol. 62, no. 12, pp. 6027–6039, Dec. 2014.
[14] Z.-J. Yang, S.-Q. Xiao, L. Zhu, B.-Z. Wang, and H.-L. Tu, "A circularly polarized implantable antenna for 2.4-GHz ISM band biomedical applications," *IEEE Antennas Wireless Propag. Lett.*, vol. 16, pp. 2554–2557, 2017.
[15] C. Liu, Y.-X. Guo, and S. Xiao, "A hybrid Patch/Slot implantable antenna for biotelemetry devices," *IEEE Antennas Wireless Propag. Lett.*, vol. 11, pp. 1646–1649, 2012.
[16] C. Liu, Y.-X. Guo, and S. Xiao, "Compact dual-band antenna for implantable devices," *IEEE Antennas Wireless Propag. Lett.*, vol. 11, pp. 1508–1511, 2012.
[17] L.-J. Xu, Y.-X. Guo, and W. Wu, "Dual-band implantable antenna with open-end slots on ground," *IEEE Antennas Wireless Propag. Lett.*, vol. 11, pp. 1564–1567, 2012.
[18] Y. Cho and H. Yoo, "Miniaturised dual-band implantable antenna for wireless biotelemetry," *Electron. Lett.*, vol. 52, no. 12, pp. 1005–1007, Jun. 2016.
[19] I. Gani and H. Yoo, "Multi-band antenna system for skin implant," *IEEE Microw. Wireless Compon. Lett.*, vol. 26, no. 4, pp. 294–296, Apr. 2016.
[20] C. Liu, Y.-X. Guo, H. Sun, and S. Xiao, "Design and safety considerations of an implantable rectenna for far-field wireless power transfer," *IEEE Trans. Antennas Propag.*, vol. 62, no. 11, pp. 5798–5806, Nov. 2014.
[21] Z. Chen, H. Sun, and W. Geyi, "Maximum wireless power transfer to the implantable device in the radiative near-field," *IEEE Antennas Wireless Propag. Lett.*, vol. 16, pp. 1780–1783, 2017.
[22] F.-J. Huang, C.-M. Lee, C.-L. Chang, L.-K. Chen, T.-C. Yo, and C.-H. Luo, "Rectenna application of miniaturized implantable antenna design for triple-band biotelemetry communication," *IEEE Trans. Antennas Propag.*, vol. 59, no. 7, pp. 2646–2653, Jul. 2011.
[23] A. Kiourti, J. R. Costa, C. A. Fernandes, A. G. Santiago, and K. S. Nikita, "Miniature implantable antennas for biomedical telemetry: From simulation to realization," *IEEE Trans. Biomed. Eng.*, vol. 59, no. 11, pp. 3140–3147, Nov. 2012.
[24] A. Kiourti and K. S. Nikita, "Miniature scalp-implantable antennas for telemetry in the MICS and ISM bands: Design, safety considerations and link budget analysis," *IEEE Trans. Antennas Propag.*, vol. 60, no. 8, pp. 3568–3575, Aug. 2012.
[25] A. Kiourti, J. R. Costa, C. A. Fernandes, and K. S. Nikita, "A broadband implantable and a dual-band on-body repeater antenna: Design and transmission performance," *IEEE Trans. Antennas Propag.*, vol. 62, no. 6, pp. 2899–2908, Jun. 2014.
[26] Y.-S. Chen, "Reduction of detuning effects using robust parameter design for implantable antennas," *Electron. Lett.*, vol. 51, no. 24, pp. 1971–1973, Nov. 2015.
[27] A. Kiourti and K. S. Nikita, "Numerical assessment of the performance of a scalp-implantable antenna: Effects of head anatomy and dielectric parameters," *Bioelectromagnetics*, vol. 34, no. 3, pp. 167–179, Apr. 2013.
[28] N. Vidal, S. Curto, J. M. Lopez-Villegas, J. Sieiro, and F. M. Ramos, "Detuning effects on implantable antenna at various human positions," in *Proc. 6th Eur. Conf. Antennas Propag. (EUCAP)*, Mar. 2012, pp. 1231–1234.
[29] R. Garg, P. Bhartia, I. Bahl, and A. Ittipiboon, *Microstrip Patch antenna Design Handbook*, Norwood, MA, USA: Artech House, 2001.
[30] N.-W. Liu, L. Zhu, and W.-W. Choi, "A differential-fed microstrip patch antenna with bandwidth enhancement under operation of TM_{10} and TM_{30} modes," *IEEE Trans. Antennas Propag.*, vol. 65, no. 4, pp. 1609–1614, Apr. 2017.
[31] O. Knecht, Y. Jundt, and J. W. Kolar, "Planar inverted-F antenna design for a fully implantable mechanical circulatory support system," in *Proc. IEEE Int. Conf. Ind. Technol. (ICIT)*, Mar. 2017, pp. 1366–1371.
[32] C. Xiao, K. Wei, D. Cheng, and Y. Liu, "Wireless charging system considering eddy current in cardiac pacemaker shell: Theoretical modeling, experiments, and safety simulations," *IEEE Trans. Ind. Electron.*, vol. 64, no. 5, pp. 3978–3988, May 2017.
[33] J. Choi, U. Kim, S. Lee, and K. Kwon, "Design of an implantable antenna for WBAN applications," in *Proc. IEEE Int. Workshop Antenna Technol. (iWAT)*, Mar. 2012, pp. 213–216.
[34] Y.-W. Yang, H.-L. Su, K.-H. Lin, H.-H. Lin, and C.-Y. Wu, "Spiral-like implanted antenna for biotelemetry," in *Proc. Asia Pacific Microw. Conf. Proc.*, Dec. 2012, pp. 409–411.
[35] Z.-J. Yang, L. Zhu, and S. Xiao, "An implantable circularly polarized patch antenna design for pacemaker monitoring based on quality factor analysis," *IEEE Trans. Antennas Propag.*, vol. 66, no. 10, pp. 5180–5192, Oct. 2018.
[36] A. D. Yaghjian and S. R. Best, "Impedance, bandwidth, and q of antennas," *IEEE Trans. Antennas Propag.*, vol. 53, no. 4, pp. 1298–1324, Apr. 2005.
[37] G. A. Mavridis, D. E. Anagnostou, and M. T. Chryssomallis, "Evaluation of the quality factor, Q, of electrically small microstrip-patch antennas [Wireless Corner]," *IEEE Antennas Propag. Mag.*, vol. 53, no. 4, pp. 214–216, Aug. 2011.
[38] S. H. Makarov, G. M. Noetscher, V. Makarov, and A. Nazarian, "Dual antiphase antenna for better signal transmission into human body or signal reception from human body," U.S. Patent 16 502 346, Oct. 24, 2019. [Online]. Available: http://www.freepatentsonline.com/y2019/0326666.html

ZHI-JIE YANG (Member, IEEE) was born in Sichuan, China, in 1990. He received the B.S. degree in the physics from Sichuan Normal University, Chengdu, China, in 2012, and the Ph.D. degree in radio physics from the University of Electronic Science and Technology of China (UESTC), Chengdu, in 2019. From March 2017 to December 2017, he was with the University of Macao, Macau, as a Research Assistant. His current research interests include microstrip antenna and implantable antenna.

LEI ZHU (Fellow, IEEE) received the B.Eng. and M.Eng. degrees in radio engineering from the Nanjing Institute of Technology (now Southeast University), Nanjing, China, in 1985 and 1988, respectively, and the Ph.D. degree in electronic engineering from the University of Electro-Communications, Tokyo, Japan, in 1993.

From 1993 to 1996, he was a Research Engineer with Matsushita-Kotobuki Electronics Industries Ltd., Tokyo. From 1996 to 2000, he was a Research Fellow with the École Polytechnique de Montréal, Montréal, QC, Canada. From 2000 to 2013, he was an Associate Professor with the School of Electrical and Electronic Engineering, Nanyang Technological University, Singapore. He joined the Faculty of Science and Technology, University of Macao, Macau, as a Full Professor, in August 2013, and has been a Distinguished Professor, since December 2016. From August 2014 to August 2017, he served as the Head of Department of Electrical and Computer Engineering, University of Macao. He has authored or coauthored more than 580 articles in international journals and conference proceedings. His articles have been cited more than 9800 times with the H-index of 51 (source: Scopus). His research interests include microwave circuits, planar antennas, periodic structures, and computational electromagnetics.

Dr. Zhu was an Associate Editor for the IEEE TRANSACTIONS ON MICROWAVE THEORY AND TECHNIQUES, from 2010 to 2013, and the IEEE MICROWAVE AND WIRELESS COMPONENTS LETTERS, from 2006 to 2012. He served as the General Chair for the 2008 IEEE MTT-S International Microwave Workshop Series on the Art of Miniaturizing RF and Microwave Passive Components, Chengdu, China, and a Technical Program Committee Co-Chair for the 2009 Asia–Pacific Microwave Conference, Singapore. He served as the member for the IEEE MTT-S Fellow Evaluation Committee, from 2013 to 2015, and as the member for the IEEE AP-S Fellows Committee, from 2015 to 2017. He was a recipient of the 1997 Asia–Pacific Microwave Prize Award, the 1996 Silver Award of Excellent Invention from Matsushita-Kotobuki Electronics Industries Ltd., and the 1993 First-Order Achievement Award in Science and Technology from the National Education Committee, China.

SHAOQIU XIAO (Member, IEEE) received the Ph.D. degree in electromagnetic field and microwave technology from the University of Electronic Science and Technology of China (UESTC), Chengdu, China, in 2003. From January 2004 to June 2004, he joined UESTC as an Assistant Professor. From July 2004 to March 2006, he worked with the Wireless Communications Laboratory, National Institute of Information and Communications Technology of Japan (NICT), Singapore, as a Research Fellow with the focus on the planar antenna and smart antenna design and optimization. From July 2006 to June 2010, he worked with UESTC as an Associate Professor. He is currently working with UESTC as a Professor. He visited Ecole Normale Superieure de Cachan, Paris, France, as a Senior Research Scholar, from July 2015 to August 2015. He has authored/coauthored more than 300 technical journals articles, conference papers, books, and book chapters. His current research interests include planar antenna and phased array, computational electromagnetics, microwave passive circuits, and time reversal electromagnetics.